

pubs.acs.org/ac Article

Photothermal Backscatter Interferometry for Enhanced Detection in Capillary Electrophoresis

Prabhavie M. Opallage,[#] Miyuru De Silva,[#] Stanslaus M. Kariuki, Armina A. Raheel, and Robert C. Dunn*



Cite This: Anal. Chem. 2024, 96, 13234-13241

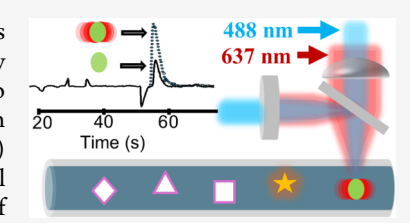


ACCESS

III Metrics & More

Article Recommendations

ABSTRACT: Refractive index (RI) detection using backscatter interferometry (BSI) enables universal detection in capillary electrophoresis (CE). BSI detection is a versatile on-capillary approach that is easily integrated with capillary or microfluidic channels, straightforward to miniaturize, and inexpensive. The focused BSI light source can also double as the excitation source for fluorescence, enabling simultaneous universal (BSI) and specific (fluorescence) signals from the same detection volume. To improve BSI detection and expand orthogonal content, we integrate photothermal absorption with BSI detection. Nonradiative relaxation of an excited analyte releases heat into the surroundings, which modifies both the local RI and



conductivity (viscosity) of the analyte zone. We recently showed that the BSI signal is sensitive to both RI and conductivity, which makes photothermal absorption a promising route to signal enhancement. Here, we use coaxially delivered BSI and photothermal absorption beams to characterize BSI, photothermal BSI, and fluorescence detection using the separation of test samples. We show that photothermal absorption leads to 3 orders of magnitude improvement in BSI detection limits at the powers studied and provides new opportunities for studying binding interactions with CE.

■ INTRODUCTION

Capillary electrophoresis (CE) is a relatively simple, flexible, and inexpensive analytical separation technique that enables rapid analysis of complex mixtures. 1-4 In CE, electrophoretic separations are carried out in a small-bore capillary to reduce Joule heating arising from the high separation voltages. While the small-bore capillary has advantage for reducing sample and reagent requirements, it presents significant challenges for analyte detection. The limited detection volume and small path length place increased demands on the detection system used to quantify analytes. 6,7

For on-capillary detection, optical methods such as laser-induced fluorescence (LIF) and UV detection have proven extremely powerful. LIF enables very low detection limits but requires the analyte be naturally fluorescent or amenable to functionalization with a fluorophore. UV detection, on the other hand, is more generally applicable since many analytes absorb in the UV, but has less favorable detection limits. Both schemes can be used in an indirect detection format for universal detection of analytes, but this comes at the expense of performance. 6,15,16

For on-capillary universal detection, methods based on conductivity and refractive index (RI) sensing have been the most widely applied. Detection based on conductivity, in particular, has become widely adopted with the introduction of capacitively coupled contactless conductivity detection (C⁴D). This approach enables conductivity detection using electrodes placed outside the capillary, increasing the

ease and flexibility of the method. While C⁴D has been widely used to detect inorganic ions and small organic ions, it is not well suited for protein and macromolecule analysis. ¹⁹ RI detection, on the other hand, can detect the full range of analytes and is easily integrated with CE. ^{20,21} This detection method, however, is less widely used due to its modest sensitivity and susceptibility to environmental influences, such as temperature fluctuations. ^{6,22,23}

RI detection in CE using backscatter interferometry (BSI) is straightforward to implement, inexpensive, readily miniaturized, and can easily be adapted for simultaneous fluorescence detection. ^{21,24–26} Moreover, we have shown that BSI detection in CE is capable of low micromolar and even high nanomolar detection limits under favorable conditions. ²⁰ This is comparable to C⁴D, but still orders of magnitude less than that routinely obtained with fluorescence detection. There are, however, approaches that can be used to enhance BSI detection.

We recently showed that the BSI signal is sensitive to the applied separation field and linearly increases with the square of the separation voltage.²² This can be exploited by using high

Received: May 2, 2024 Revised: July 17, 2024 Accepted: July 23, 2024 Published: July 29, 2024





separation voltages to enhance BSI detection.²⁷ This approach, however, is ultimately limited by Joule heating which degrades separation performance. Here, we explore the integration of photothermal processes to expand the capabilities of BSI detection in CE.

The photothermal or thermal lensing effect is a well-established approach for improving the sensitivity of absorbance measurements in small volumes. $^{28-32}$ In this method, an excitation beam is focused into the sample to resonantly excite an analyte. Nonradiative relaxation back to the ground state releases heat into the surroundings and creates a local RI gradient in the solvent. For a laser beam focused into an absorbing sample, the intensity profile leads to the lensing effect. Since most common solvents have a negative thermo-optic coefficient (dn/dt), heating results in the generation of a negative thermal lens element in the optical path. 29 The thermal lens created in the sample is commonly probed using a second probe beam passing through the perturbed region. $^{33-35}$

Various geometries and schemes have been introduced for photothermal detection in separations. These include both single and dual beam detection schemes using both coaxial and crossed beam geometries. ^{28–30,33,36} Dual beam detection, where a weak probe beam is used to interrogate the thermal lens created by a stronger excitation beam, has shown to offer many advantages over the simpler single beam approach. The dual beam method, for example, lends itself to sensitive lock-in detection where the excitation beam is modulated. Second, both theoretical and experimental studies have shown the advantage of using a mode-mismatched geometry, where the waist of the excitation beam is centered in the sample while that of the probe is offset. ^{33,34,36} This arrangement is not possible in the single beam approach.

The thermal lens enhancement goes as $P(dn/dT)k\lambda$ where P and λ are the laser power (Watts) and wavelength, respectively; and dn/dT and k are the thermo-optic coefficient and thermal conductivity (W cm⁻¹ K⁻¹)of the solvent, respectively.²⁹ Unfortunately, for detection in CE, water is a particularly poor solvent for thermal lens enhancement given its relatively small thermo-optic coefficient ($-0.8 \times 10^{-4} \text{ K}^{-1}$) and large thermal conductivity (6.11 mW cm⁻¹ K⁻¹).²⁸ Nevertheless, the enhancement scales with excitation power and overtakes linear absorption in aqueous solutions with only a few milliwatts of excitation (4.2 mW at 632.8 nm).³³

Nonaqueous solvents can also be used to improve the thermal lens enhancement, where $(\mathrm{d}n/\mathrm{d}T)k$ can be an order of magnitude larger than that for water. Organic solvents like carbon tetrachloride and acetone, for example, have ratios of -0.57 and -0.31 cm/W, respectively, compared to that of water which is -0.013 cm/W.²⁹ For applications in CE, however, nonaqueous solvents have limited practical value.

The modest thermo-optic effect has led to the exploration of other detection signals for CE that can be enhanced through photothermal absorption. Solvent viscosity is sensitive to temperature, which suggests that conductivity detection in CE could benefit.^{37–39} It was recognized early that the change in viscosity with temperature for water is orders of magnitude larger than the RI change, suggesting a promising route for enhanced CE detection.³⁷ In fact, a study integrating photothermal absorbance with C⁴D detection measured an ~20-fold increase in signal.³⁹ While clearly enhanced, the magnitude was less than expected. It was determined that the mismatch between the localized volume heated photothermally

and the larger sensing region of the C^4D detector lowered expected signal levels. To overcome this, recent studies have revisited using contacting electrodes for detection in microfluidic devices. While electrodes in contact with the solution are more efficiently coupled with photothermal absorption, they present significant obstacles for integration with capillary based techniques.

We recently showed that the BSI signal in CE is composed of two components. One term responds to the RI of the analyte zone as expected, but a second term responds to the conductivity of the analyte zone.²⁷ The latter leads to the squared voltage dependence in the BSI signal mentioned earlier.^{22,27} The sensitivity of the BSI signal to both RI and conductivity of the analyte zone raises intriguing possibilities for enhancing BSI detection through photothermal absorption.

Herein, we integrate photothermal absorption with BSI detection in CE to simultaneously measure RI, photothermal absorption, and fluorescence signals. Using multiple laser lines coupled into a shared fiber optic, we use coaxial excitation and probe beams to explore the utility of photothermal enhancement. Our results show that photothermal absorption probed with BSI enables analyte detection down to the nanomolar level. The selective excitation of analytes during a separation can help identify and enhance their signals, and preliminary measurements are presented that show the utility of this approach for measuring binding interactions in CE.

METHODS AND MATERIALS

Chemicals. Sodium chloride, potassium chloride, lithium chloride, brilliant green (BG), bromocresol green (BCG), imidazole, sodium hydroxide, and rhodamine 123 (R123) were obtained from Fisher Scientific (Fair Lawn, New Jersey) and used without further purification. Human serum albumin (HSA) and boric acid were obtained from Sigma-Aldrich (St Louis, Missouri) and used as received. HSA solutions at the indicated concentrations were made the same day of use.

Imidazole and boric acid buffer background electrolytes (BGEs) were made at the appropriate concentrations, and their pH adjusted with the addition of concentrated HCl or NaOH as required. A stock solution 1 mM each in Na⁺, K⁺, and Li⁺ was prepared and diluted as required to prepare samples. Stock solutions of 200 μ M BG and 200 μ M R123 were prepared and diluted as necessary to make the test samples. All solutions were prepared and diluted using ultrapure water as the solvent and filtered through a 0.22 μ m filter (Fisher Scientific, New Jersey). The solutions were stored at 4 °C and allowed to equilibrate to room temperature prior to use.

Experimental Apparatus. The home-built planar capillary electrophoresis (PCE) platform has been described previously. $^{20-22,24}$ Briefly, the PCE uses a 10 cm total length fused silica capillary (VitroCom, 50 μ m i.d. \times 80 μ m o.d.) with an 8 cm length-to-detector. To facilitate heat dissipation, the capillary is mounted flush on a heat sink and its length covered with a thermal paste, except for small regions located at the detection window and near the capillary ends. An O-ring enclosure seals against the capillary outlet and under-pressures are applied to flush fluids through the capillary for conditioning. At the capillary inlet, appropriate solutions are held in small vials which are positioned at the inlet using a rotating platform driven by a computer-controlled stepper motor. Separation voltage from a Spellman CZE 2000 is supplied to a Pt electrode in contact with solutions positioned

at the capillary inlet. The PCE is mounted on an inverted fluorescence microscope (Zeiss Axio, Baden-Württemberg, Germany), and the detection zone of the capillary is aligned above the microscope objective (0.15 NA, 5x Zeiss N-Achroplan) of the microscope.

For BSI detection, the appropriate laser line is coupled into a single mode optical fiber (ThorLabs, SM450). The output of the optical fiber is held in a custom-built mount which integrates a collimating lens and focusing lens (singlet, 40 mm FL). The optical assembly is held in a high precision 3-axis translation stage (Linetool Model A LHFF, Allentown PA) to align the focused laser beam into the detection zone of the capillary. A 45° broadband (400-700 nm) 50% beam splitter (Edmund Optics, 48-902) placed between the focusing lens and the capillary reflects backscattered light from the capillary toward a split photodiode detector. Appropriate fringes in the BSI pattern are aligned on a split photodiode detector and the two outputs are differentially amplified (Stanford Research Systems, SR560) to generate the BSI signal. All signal collection and instrument controls are interfaced through a data acquisition device (National Instruments, USB-6001) using custom software written in LabView (National Instruments).

Three laser sources are coupled into a single mode fiber to provide photothermal and BSI excitation. Spectra-Physics Cyan (488 nm, 20 mW; Milpitas CA), Research Electro-Optics HeNe (543 nm, 2 mW; Boulder CO), and Coherent Obis (637 nm, 140 mW; Santa Clara CA) lasers were utilized. For modulated photothermal measurements, the output power of the Obis laser was modulated using a sine wave generated with a function generator (8116A; Hewlett-Packard, Palo Alto CA). The signal outputs from the split photodiode detector were sent to a lock-in amplifier (Stanford Research Systems, SR560) referenced to the function generator. For fluorescence measurements, light collected with the microscope objective is filtered (Chroma Technology, Vermont USA) to remove excitation and photothermal sources, and the fluorescence is detected on a PMT (01–612, Photon Technology).

■ RESULTS AND DISCUSSION

In planar capillary electrophoresis (PCE), RI detection using BSI utilizes the optical path shown schematically in Figure 1A.

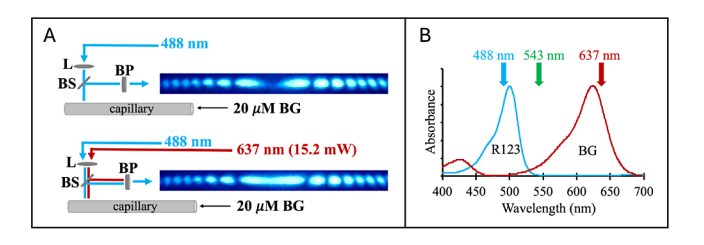


Figure 1. (A) Comparison of a BSI patterns generated with 488 nm light, measured in the absence (upper) and presence (lower) of photothermal absorption of a 20 μ M BG solution that is passed through the capillary using pressure. Light from a 488 nm laser is focused with a lens (L) through a beamsplitter (BS) and into the detection zone of the capillary. Backscattered light from the capillary reflects from the BS and through a bandpass filter (BP) to yield the BSI pattern shown in the top image. With coaxial photothermal absorption of BG using 15.2 mW of 637 nm (bottom image), a large shift in the BSI pattern is observed. (B) Absorption spectra of rhodamine 123 (R123) and brilliant green (BG). Arrows denote the laser lines used in this study.

A collimated laser source is focused through a 45° dichroic beam splitter and into the detection zone of the separation capillary. The backscattered interference pattern from the capillary is reflected off the beam splitter, sent through a bandpass (BP) filter, and directed onto a detector as described elsewhere. 20,22,25

The top image in Figure 1A shows a typical BSI interference pattern measured using excitation from a 488 nm single frequency laser (Spectra Physics Cyan Laser).²⁵ As discussed previously, the interference pattern is sensitive to changes in solution RI and shifts in response to analyte zones passing through the capillary. 42,43 The BSI pattern was collected while flowing a 20 µM solution of brilliant green (BG) through the capillary using an under pressure applied at the capillary outlet. The spectrum of BG is shown in Figure 1B and exhibits a strong absorption maximum located near 625 nm that goes to baseline at 488 nm. The 488 nm BSI pattern in Figure 1A (top image), therefore, reflects the RI of the solution with little to no excitation of BG. To demonstrate the feasibility of photothermal BSI, the lower image in Figure 1A shows the 488 nm BSI pattern when BG is simultaneously excited with 637 nm light. Here, excitation from a 637 nm laser (Coherent Obis) is coaxially delivered with the 488 nm line used for BSI detection. The 637 nm light optically excites the BG in solution, leading to the large photothermal shift in BSI pattern as shown in Figure 1A.

To explore photothermal absorption in PCE-BSI, a test sample mixture of K⁺, Na⁺, Li+ (50 μ M each), rhodamine 123 (R123, 25 μ M), and BG (50 μ M) was prepared. The spectra of both R123 and BG are shown in Figure 1B along with the three laser lines used in this study. As shown schematically in Figure 2A, the three laser sources are coupled into a single

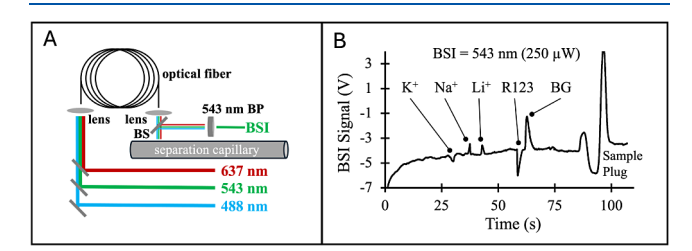


Figure 2. (A) Optical path used for coaxial BSI and photothermal absorption. Three laser lines are coupled into a single mode fiber. The collimated output of the fiber uses the same optical path as that discussed in Figure 1. Initial experiments used the 543 nm line for BSI detection while the 488 and 637 nm lines were used for selective photothermal absorption of R123 and BG, respectively (Figure 1A). (B) Typical 543 nm BSI electropherogram of a test mixture containing K⁺ (50 μ M), Na⁺ (50 μ M), Li⁺ (50 μ M), R123 (25 μ M), and BG (50 μ M) separated in a 20 mM imidazole buffer at pH 6.2. For this electropherogram, the separation voltage was 3 kV (300 V/cm) and an electrokinetic sample injection at 4 kV for 1 s was utilized.

mode optical fiber. The output of the fiber provides a common optical path for the three laser lines to the capillary detection zone. This enables coaxial photothermal and BSI excitation using any combination of the three laser lines. Mode mismatched coaxial laser beams have been found to provide the optimal configuration for photothermal studies. ^{34,36} As shown previously, the chromatic aberration in a shared focusing element inherently leads to mode mismatch over a

wide range of conditions.³³ This approach, therefore, is easy to implement and robust.

For the initial studies, the 543 nm HeNe laser line was used to generate the BSI signal while the 488 and 637 nm laser lines specifically excite R123 and BG, respectively. As shown in Figure 1B, the 543 nm laser line is located at an absorption minimum between the R123 and BG maxima and thus contributes minimally to any photothermal processes. The backscattered interference fringes are aligned on a split photodiode and the differentially amplified output recorded as the BSI signal. 20-22,25,27,44 A 543 nm bandpass filter is placed before the detector to block scattered light from the 488 and 637 nm excitation beams, as shown in Figure 2A. Figure 2B shows a full electropherogram for the five analytes separated in a 20 mM imidazole buffer at pH 6.2. The electropherogram was measured using the 543 nm BSI signal with both 488 and 637 nm beams blocked during collection. All analytes are detected with the universal BSI signal within 70 s of injection using a separation voltage of 3000 V (300 V/cm). The large, saturating signal near 100 s arises from the migrating sample plug. This neutral zone arising from the water used to prepare samples provides a convenient marker of electroosmotic flow (EOF) in each separation.⁴⁵

Electropherograms are shown in Figure 3 that summarize the effects of selective excitation of R123 or BG using 488 or

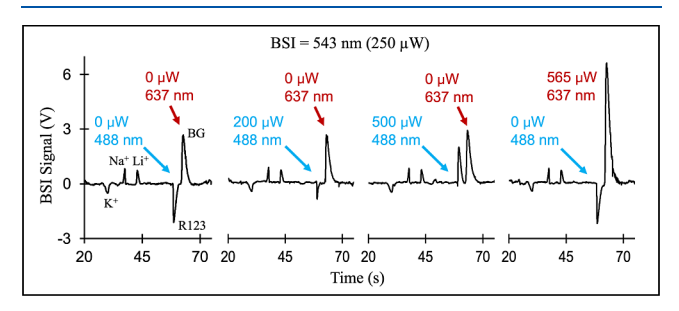


Figure 3. A series of electropherograms showing only the peaks of interest. These 20–75 s regions were extracted from full electropherograms like that shown in Figure 2B and have been background subtracted. The first three electropherograms show the effects of selective photothermal absorption of R123 with 488 nm while the fourth shows the selective enhancement of BG with 637 nm excitation. Photothermal absorption leads to BSI signals becoming more positive, which leads to the change in sign observed for the R123 peak. Separation conditions: BGE, 20 mM imidazole at pH 6.2; separation voltage, 3 kV (300 V/cm); electrokinetic sample injection, 1 s at 4 kV.

637 nm, respectively. Using the same separation conditions as that in Figure 2B, these 20–75 s regions of interest have been extracted from the full electropherograms and background subtracted to remove the slow rise in BSI signal observed in Figure 2B.

The first electropherogram in Figure 3 shows the analyte peaks in the absence of any other excitation. The second and third electropherograms show the effects of selective excitation of R123 at 488 nm. Excitation with 200 μ W of 488 nm reduces the amplitude of the negative going R123 peak. As the power is increased to 500 μ W, the peak changes sign to a positive going peak with large amplitude. Even though R123 is a fluorescent dye with a fluorescence quantum yield of 0.90, 46 nonradiative relaxation still significantly alters the photothermal BSI signal.

Photothermal absorption leads to local heating which lowers the RI and increase the conductivity of the analyte zone. As we recently reported, both mechanisms contribute to the BSI signal. In the absence of photothermal absorption, the magnitude of each contribution can lead to negative or positive going analyte peaks at a given separation voltage. Regardless of the initial peak direction, here photothermal absorption will always pull the peak toward the positive side. This is confirmed in the last electropherogram in Figure 3, which shows the effects of selective excitation of BG with 637 nm. Coaxial excitation with 565 μ W at 637 nm significantly increases the amplitude of the positive going BG peak. Neither excitation source appears to affect the other nonresonant dye molecule in the separation and we observe no change in the inorganic ion peak amplitudes at these excitation powers. The series of electropherograms in Figure 3, therefore, show that the photothermal peak enhancement is specific and can be significant.

To characterize the effects of photothermal absorption power, a simpler two beam arrangement was used with 488 and 637 nm coupled into the optical fiber. The BSI signal is generated using the 488 nm (850 μ W) laser line while excitation power from the 637 nm laser is varied to excite BG. For these experiments, a short pass filter was placed before the detector to pass 488 nm and block 637 nm light. Using the same test sample mixture and separation conditions, Figure 4 summarizes the results.

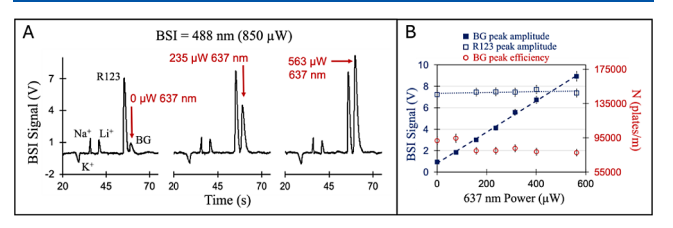


Figure 4. (A) Representative electropherograms of the test mixture where the BSI signal is generated using the 488 nm laser line (850 μ W) and the BG peak is increasingly enhanced using photothermal absorption at 637 nm. The large positive going peak for R123 results from the BSI laser (488 nm) doubling as the excitation source for R123. (B) A plot of BG peak amplitude versus 637 nm excitation power results in the linear trend shown. BG peak efficiency is also relatively flat across the power range studied as is the peak amplitude for the neighboring R123 peak. Separation conditions: BGE, 20 mM imidazole at pH 6.2; separation voltage, 3 kV (300 V/cm); electrokinetic sample injection, 1 s at 4 kV.

The large positive going peak for R123 results from its photothermal absorption from the 488 nm line, which is now being used to generate the BSI signal. This is equivalent to a single beam, mode-matched arrangement for R123 photothermal absorption. Similarly, the BG peak in Figure 4A is reduced compared to the electropherograms shown in Figures 2 and 3 since BG absorbs less at 488 nm (see Figure 1B). The representative electropherograms in Figure 4 show that as the 637 nm excitation power is increased, the peak for BG grows in magnitude while the other peaks in the electropherogram remain unaffected. Electropherograms were measured using 637 nm powers ranging from 0 to 563 μ W. Key parameters extracted from the electropherograms are plotted in Figure 4B. In agreement with previous work, the BG peak height increases linearly with 637 nm excitation power.²⁹ The plot of BG peak efficiency shows an initial drop, followed by relatively constant values across the excitation power range studied. Finally, to probe any "spillover" effects on neighboring peaks or

nonresonant enhancements, the peak amplitude for R123 is plotted with 637 nm excitation power. The relatively constant response indicates these effects are minimal under these conditions.

The results shown in Figures 3 and 4 illustrate the selective peak enhancement that can be obtained through photothermal absorption. To explore the improvement in detection limits, Figure 5 presents electropherograms measured at reduced

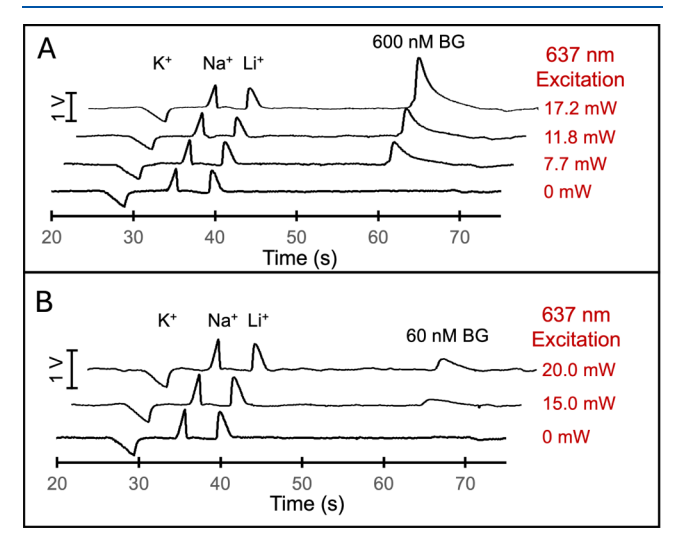


Figure 5. Electropherograms of a sample mixture containing K⁺ (50 μ M), Na⁺ (50 μ M), Li⁺ (50 μ M), and BG at levels of (A) 600 nM and (B) 60 nM. The mixture was separated in 20 mM imidazole at pH 6.2 and the BSI signal generated using 488 nm light. In (A), the 600 nM level of BG is not detected in the BSI signal until coaxial excitation with 637 nm enhances the peak. Panel (B) shows that BG detection down to the nanomolar level is possible with increasing 637 nm excitation power. Separation conditions: separation voltage, 3 kV (300 V/cm); electrokinetic sample injection, 1 s at 4 kV.

concentrations of BG. Figure 5A shows a series of electropherograms (BSI at 488 nm) for a sample mixture containing 50 µM each of K⁺, Na⁺, and Li⁺ and 600 nM BG. In the absence of 637 nm excitation, only the three inorganic ion peaks are detected in the BSI signal. As the 637 nm power is increased from 7.7 to 17.2 mW, however, the analyte peak due to BG begins to appear and grows in amplitude. Figure 5B shows similar electropherograms for a sample mixture consisting of the same 50 μ M each of K⁺, Na⁺, Li⁺, but with the BG level reduced another order of magnitude to 60 nM. Even at this low level, the BG peak is easily detected in the BSI signal at 637 nm excitation powers above 15 mW. In each electropherogram, the inorganic ion (K+, Na+, Li+) levels are held constant at 50 μM and are unaffected by 637 nm excitation, so their peak amplitudes remain approximately the same. These peaks provide markers to judge the effectiveness of photothermal excitation. For example, the relative peak height of 50 μ M BG in Figure 4A (no excitation) is comparable with that of 60 nM BG in Figure 5B (20.0 mW excitation), suggesting an estimated improvement in signal of 3 orders of magnitude. Even lower detection limits should be possible at higher laser powers.

One advantage of BSI compared to nonoptical universal detectors is the ease with which fluorescence can be added as an orthogonal detection signal. This is demonstrated using a sample mixture containing 50 μ M each of K⁺, Na⁺, and

Li⁺, 60 nM BG, and 60 nM the fluorescent dye R123. The same coaxial 488 nm/637 nm excitation geometry is used with the 488 nm line now serving as both the BSI signal and excitation source for R123 fluorescence. Fluorescence is collected from below the capillary using a microscope objective (0.15 NA, 5x Zeiss Achroplan), filtered through a bandpass filter to remove residual 488 and 637 nm excitation, and detected on a photomultiplier tube.

Figure 6A shows the simultaneously collected BSI and fluorescence electropherograms of the sample mixture using

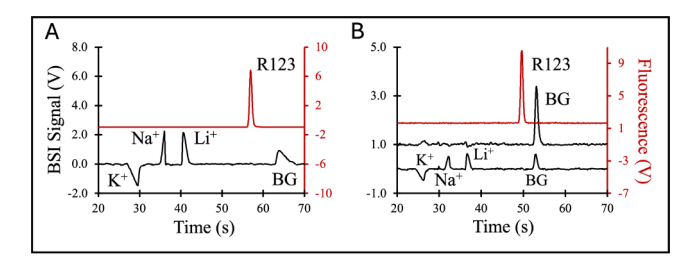


Figure 6. (A) Simultaneously measured BSI and fluorescence electropherograms of a sample mixture containing K⁺ (50 μ M), Na⁺ $(50 \ \mu\text{M})$, Li⁺ $(50 \ \mu\text{M})$, R123 $(60 \ \text{nM})$, and BG $(60 \ \text{nM})$. The BSI electropherogram generated using 488 nm light detects the inorganic ions and the 60 nM BG using photothermal absorption at 637 nm. The 488 nm laser line generates the BSI signal and excites fluorescence from the 60 nM R123, which is not visible in the BSI electropherogram, while 20 mW coaxial excitation at 637 nm enhances and makes visible the 60 nM BG peak in the BSI signal. (B) Simultaneously measured fluorescence (top), modulated BSI (middle), and BSI (bottom) electropherograms of a K^+ (50 μ M), Na^+ (50 μ M), Li⁺ (50 μ M), R123 (60 nM), and BG (600 nM) sample mixture. For the modulated BSI signal, the photothermal absorption at 637 nm is modulated at 500 Hz and the signal detected using a lock-in amplifier. Separation conditions: BGE, 20 mM imidazole at pH 6.2; separation voltage, 3 kV (300 V/cm); electrokinetic sample injection, 1 s at 4 kV.

the same separation conditions as before. In the BSI electropherogram, the K^+ , Na^+ , and Li^+ analytes (50 μM each) are detected by the BSI signal while the BG peak (60 nM) is visible from photothermal absorption (20 mW at 637 nm). In the fluorescence electropherogram, a single peak from R123 (60 nM) is measured with a migration time consistent with previous measurements (see Figure 3). Since all signals arise from the same 488 nm excitation, the same detection volume is probed and the electropherograms are perfectly registered with each other.

Most previous two beam photothermal studies have used a signal modulation scheme to improve signal-to-noise. Modulating the 637 nm photothermal absorption beam, for example, leads to a modulated BSI signal for the BG peak, which lends itself lock-in detection. The addition of this channel is shown in Figure 6B. In these experiments, the 637 nm laser power was electronically modulated (0 to 3 mW) using a sine wave at 500 Hz. The modulated BSI signal was detected using a lock-in amplifier and the output was recorded as the photothermal electropherogram. For these measurements, the sample consisted of 50 μ M each of K⁺, Na⁺, and Li⁺, 600 nM BG, and 60 nM R123.

The three simultaneously collected electropherograms are shown in Figure 6B. As before, the fluorescence electropherogram contains a single peak due to the fluorescence from R123 (60 nM). The BSI electropherogram contains peaks associated

with K⁺, Na⁺, and Li⁺ (50 μ M each) and the photothermally enhanced BG (600 nM). The middle electropherogram shows the signal from the lock-in amplifier which contains one peak due to the modulated excitation of BG. Surprisingly, preliminary studies using modulation frequencies ranging from 50 Hz to 1 kHz did not result in a significant improvement in signal-to-noise over direct excitation measurements. This may be linked with slow heat dissipation from the separation capillary and further experiments are currently underway to understand and fully optimize this approach.⁴⁷

As shown in the previous figures, photothermal absorption combined with BSI detection can improve both the selectivity and sensitivity of analyte detection in PCE-BSI separations. Photothermal signal enhancement may also provide new opportunities for studying binding interactions with CE. This is especially important for situations where bound and unbound species are not resolved in the electropherograms. To demonstrate these capabilities, dye binding to human serum albumin (HSA) is measured.

HSA is involved in a wide range of functions and abnormal levels can reflect conditions ranging from malnutrition and dehydration to liver disease. Clinically, serum levels of HSA are normally quantified using a colorimetric assay that measures the binding of the anionic dye, bromocresol green (BCG), to HSA. Here we are using this system to demonstrate that binding interactions can be detected using photothermal absorption, even when bound and unbound peaks are not resolved in the electropherograms. BCG is a pH indicator with pK_a of 4.8 and Figure 7A shows the absorption

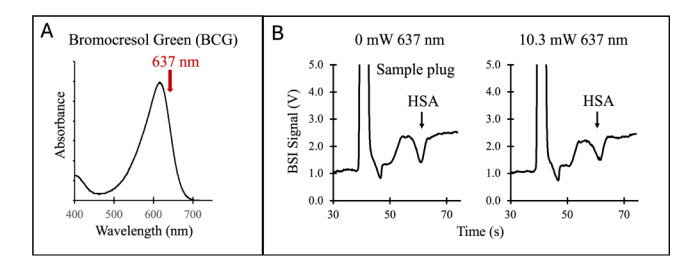


Figure 7. (A) Absorption spectrum of bromocresol green (BCG). (B) BSI electropherograms of human serum albumin (HSA) separated in 15 mM boric acid buffer at pH 10. The negatively charged HSA migrates after the sample plug which migrates with the EOF. In the absence of BCG, excitation at 637 nm leads to a small decrease in the HSA peak amplitude. Separation conditions: separation voltage, 3 kV (300 V/cm); electrokinetic sample injection, 1 s at 5 kV.

spectrum of BCG in water, which has a strong absorbance centered near 610 nm. HSA does not absorb significantly in this spectral region so binding of BCG to HSA should induce a photothermal enhancement for the protein/dye complex in the electropherogram upon excitation at 637 nm.

Figure 7B shows BSI (488 nm) electropherograms for HSA (4.5 mg/mL) separated in a BGE of 15 mM boric acid at pH 10.0. For these measurements, the BCG dye was not present in the solution and the electropherograms have not been processed to remove the background. The negatively charged HSA peak migrates after the sample plug, which marks the EOF. The small negative going peak immediately after the sample plug is assigned to a contaminant or system peak and the subsequent rise in BSI signal before the HSA peak is associated with the elution of the sample plug from the end of the capillary.

The electropherograms in Figure 7B were measured in the absence and presence of coaxial excitation with 637 nm. A slight decrease in the amplitude of the HSA peak is observed as the 637 nm excitation is increased to 10.3 mW. Even though the solution is transparent at this wavelength, a small amount of sample heating at this power is detected in the BSI signal for the HSA peak.³⁷

A HSA solution (10 mg/mL) was incubated with BCG (1 mM) for 2 h and separated in 15 mM boric acid at pH 10.0. The resulting electropherograms as a function of 637 nm excitation power are shown in Figure 8A. As the 637 nm

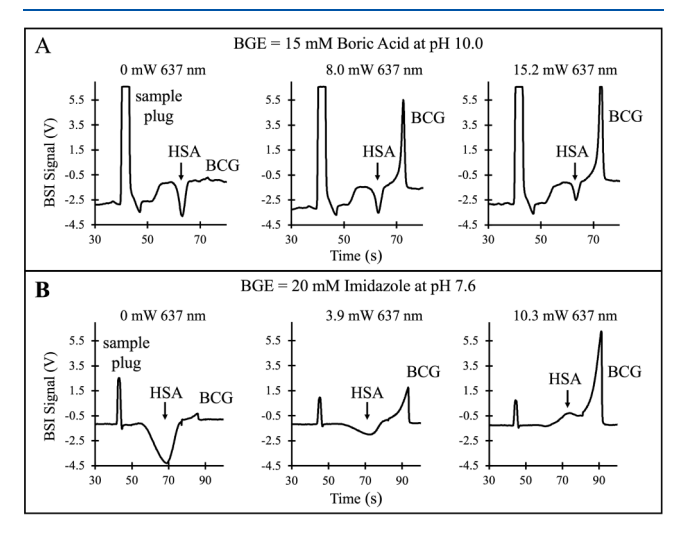


Figure 8. (A) BSI electropherograms of HSA incubated with BCG and separated in 15 mM boric acid at pH 10.0. As photothermal absorption of BCG with 637 nm is increased, both the BCG peak increases and the HSA peak decreases, indicating binding of BCG to HSA. (B) BSI electropherograms of HSA incubated with BCG and separated in 20 mM imidazole at pH 7.6. As excitation at 637 nm increases, a large decrease and eventual reversal in the HSA peak is observed. This shows that BCG is binding to HSA and leads to a large photothermal enhancement in the BSI signal. Separation conditions: separation voltage, 3 kV (300 V/cm); electrokinetic sample injection, 1 s at 5 kV.

excitation power is increased, the peak associated with the negatively charged BCG dye grows in intensity as expected. Interestingly, the magnitude of the HSA peak decreases as the power increases, suggesting a photothermal effect from binding of BCG to HSA. This is confirmed in experiments carried out in a lower pH, where binding is expected to be more favorable. ⁵⁰

Figure 8B presents electropherograms of the HSA/BCG mixture measured in a BGE of 20 mM of imidazole at pH 7.6. The electropherogram measured in the absence of 637 nm excitation shows that the HSA peak efficiency is reduced in the lower pH BGE, likely due to wall interactions that become more prevalent. As the 637 nm power is increased to 3.6 mW, the amplitude of the HSA peak dramatically reduces indicating the presence of BCG binding to HSA. This is accompanied by the expected growth in the BCG peak due to photothermal absorption. Further increasing photothermal absorption to 10.3 mW leads to a reversal in the HSA complex peak from negative going to positive going. The large photothermal response of the HSA peak reflects the binding of BCG, which would be difficult to unambiguously assign using other parameters like migration time.

CONCLUSIONS

Photothermal absorption is combined with BSI detection in PCE to enhance selectivity and sensitivity. BSI and photothermal absorption beams are delivered coaxially to probe sample mixtures containing inorganic ions (Na+, K+, and Li+) and dye molecules (BG and R123). Selective photothermal absorption of each dye leads to a linear increase in peak amplitude with excitation power, while not influencing other analyte peaks in the electropherogram. BSI detection of BG is shown to improve detection by 3 orders of magnitude in the presence of photothermal absorption. Access to higher excitation powers is expected to further improve detection limits. Using the same excitation geometry, we show that it is straightforward to simultaneously measure RI, photothermal absorption, and fluorescence signals from the same detection volume in one separation. This leads to perfectly registered, complementary electropherograms of orthogonal signals. Finally, using the well-known binding of BCG to HSA, we show how selective photothermal absorption can aid in the study of binding interactions with CE. The increased selectivity, improved detection limits and ability to probe binding interactions using photothermal absorption greatly expands the applications accessible with BSI detection.

AUTHOR INFORMATION

Corresponding Author

Robert C. Dunn — Ralph N. Adams Institute for Bioanalytical Chemistry, Department of Chemistry, University of Kansas, Lawrence, Kansas 66047, United States; orcid.org/0000-0002-6632-9736; Email: rdunn@ku.edu

Authors

Prabhavie M. Opallage — Ralph N. Adams Institute for Bioanalytical Chemistry, Department of Chemistry, University of Kansas, Lawrence, Kansas 66047, United States

Miyuru De Silva — Ralph N. Adams Institute for Bioanalytical Chemistry, Department of Chemistry, University of Kansas, Lawrence, Kansas 66047, United States

Stanslaus M. Kariuki — Ralph N. Adams Institute for Bioanalytical Chemistry, Department of Chemistry, University of Kansas, Lawrence, Kansas 66047, United States

Armina A. Raheel — Ralph N. Adams Institute for Bioanalytical Chemistry, Department of Chemistry, University of Kansas, Lawrence, Kansas 66047, United States

Complete contact information is available at: https://pubs.acs.org/10.1021/acs.analchem.4c02312

Author Contributions

*P.M.O. and M.D.S. contributed equally. The manuscript was written through contributions of all authors. All authors have given approval to the final version of the manuscript.

Notes

The authors declare no competing financial interest.

ACKNOWLEDGMENTS

We gratefully acknowledge support from the National Science Foundation (CHE-2247387) and the University of Kansas. M.D.S. acknowledges support from the Metrohm Summer Scholar program.

REFERENCES

- (1) Creamer, J. S.; Oborny, N. J.; Lunte, S. M. Anal. Methods **2014**, 6 (15), 5427–5449.
- (2) Ragab, M. A. A.; El-Kimary, E. I. Crit. Rev. Anal. Chem. 2021, 51 (8), 709-741.
- (3) Jaywant, S. A.; Singh, H.; Arif, K. M. Sens. Bio-Sens. Res. 2024, 43, 100617.
- (4) Jorgenson, J. W.; Lukacs, K. D. Science 1983, 222 (4621), 266-
- (5) Evenhuis, C. J.; Haddad, P. R. Electrophoresis 2009, 30 (5), 897-
- (6) Swinney, K.; Bornhop, D. J. Electrophoresis 2000, 21 (7), 1239–1250.
- (7) Hempel, G. Electrophoresis 2000, 21 (4), 691-698.
- (8) Huang, Y. F.; Huang, C. C.; Hu, C. C.; Chang, H. T. *Electrophoresis* **2006**, 27 (18), 3503–3522.
- (9) Galievsky, V. A.; Stasheuski, A. S.; Krylov, S. N. Anal. Chim. Acta 2016, 935, 58-81.
- (10) Hartung, S.; Minkner, R.; Olabi, M.; Wätzig, H. TrAC, Trends Anal. Chem. 2023, 163, 117056.
- (11) Cui, Y.; Jiang, Z.; Sun, J.; Yu, J.; Li, M.; Li, M.; Liu, M.; Guo, X. Food Chem. **2014**, 158, 401–407.
- (12) Nguyen, B. T.; Kang, M.-J. Molecules 2019, 24 (10), 1977.
- (13) Osbourn, D. M.; Weiss, D. J.; Lunte, C. E. Electrophoresis 2000, 21 (14), 2768–2779.
- (14) Crego, A. L.; Marina, M. L. UV-Vis absorbance detection in capillary electrophoresis. *Analysis and Detection by Capillary Electrophoresis* Elsevier 2005, 45, 225.
- (15) Wang, T.; Hartwick, R. A. J. Chromatogr. A 1992, 607 (1), 119–125.
- (16) Johns, C.; Macka, M.; Haddad, P. R. Electrophoresis 2003, 24 (12-13), 2150-2167.
- (17) Xiong, B.; Hu, J. M. Analyst 2011, 136 (4), 635-641.
- (18) Elbashir, A. A.; Elgorashe, R. E. E.; Alnajjar, A. O.; Aboul-Enein, H. Y. Crit. Rev. Anal. Chem. 2022, 52 (3), 535–543.
- (19) Tůma, P. Anal. Chim. Acta 2022, 1225, 340161.
- (20) De Silva, M.; Opallage, P. M.; Dunn, R. C. Anal. Methods **2021**, 13 (11), 1340–1348.
- (21) Opallage, P. M.; De Silva, M.; Dunn, R. C. Sci. Rep. 2022, 12, 1951.
- (22) Dunn, R. C. Anal. Chem. 2020, 92 (11), 7540-7546.
- (23) Kasyutich, V. L. Instrum. Exp. Tech. 1999, 42 (3), 423-426.
- (24) De Silva, M.; Dunn, R. C. Electrophoresis **2023**, 44 (5–6), 549–557.
- (25) Dunn, R. C. Anal. Methods 2019, 11, 2303-2310.
- (26) Wang, Z. L.; Swinney, K.; Bornhop, D. J. Electrophoresis 2003, 24 (5), 865–873.
- (27) De Silva, M.; Dunn, R. C. Sci. Rep. 2024, 14 (1), 2110.
- (28) Dovichi, N. J.; Harris, J. M. Anal. Chem. 1979, 51 (6), 728-731.
- (29) Dovichi, N. J.; Nolan, T. G.; Weimer, W. A. Anal. Chem. 1984, 56 (9), 1700–1704.
- (30) Nolan, T. G.; Weimer, W. A.; Dovichi, N. J. Anal. Chem. 1984, 56 (9), 1704–1707.
- (31) Cassano, C. L.; Mawatari, K.; Kitamori, T.; Fan, Z. H. Electrophoresis 2014, 35 (16), 2279-2291.
- (32) Bruno, A. E.; Paulus, A.; Bornhop, D. J. Appl. Spectrosc. 1991, 45 (3), 462-467.
- (33) Li, F.; Kachanov, A. A.; Zare, R. N. Anal. Chem. 2007, 79 (14), 5264–5271.
- (34) Jun, S.; Lowe, R. D.; Snook, R. D. Chem. Phys. 1992, 165 (2–3), 385–396.
- (35) Berthoud, T.; Delorme, N.; Mauchien, P. Anal. Chem 1985, 57 (7), 1216–1219.
- (36) Snook, R. D.; Lowe, R. D. Analyst 1995, 120 (8), 2051-2068.
- (37) Mclaren, R.; Dovichi, N. J. Anal. Chem. 1988, 60 (7), 730-733.
- (38) Dennis, P. J.; Welch, E. F.; Alarie, J. P.; Ramsey, J. M.; Jorgenson, J. W. *Anal. Chem.* **2010**, 82 (10), 4063–4071.

- (39) Johnston, S. E.; Fadgen, K. E.; Jorgenson, J. W. Anal. Chem. 2006, 78 (15), 5309-5315.
- (40) Chun, H.; Dennis, P. J.; Welch, E. R. F.; Alarie, J. P.; Jorgenson, J. W.; Ramsey, J. M. *J. Chromatogr. A* **2017**, *1523*, 140–147.
- (41) Xiong, B.; Wang, W.; Miao, X. Y.; Liu, L. J.; Wang, L. P.; Zhou, X. D.; Hu, J. M. *Talanta* **2012**, *88*, 168–174.
- (42) Swinney, K.; Markov, D.; Bornhop, D. J. Rev. Sci. Instrum. 2000, 71 (7), 2684–2692.
- (43) Wang, Z. L.; Bornhop, D. J. Anal. Chem. 2005, 77 (24), 7872-7877.
- (44) Dunn, R. C. Anal. Chem. 2018, 90 (11), 6789-6795.
- (45) Gas, B.; Hruska, V.; Dittmann, M.; Bek, F.; Witt, K. J. Sep. Sci. **2007**, 30 (10), 1435–1445.
- (46) Kubin, R. F.; Fletcher, A. N. J. Lumin. 1982, 27 (4), 455-462.
- (47) Proskurnin, M. A.; Bendrysheva, S. N.; Smirnova, A. P. J. Anal. Chem. **2016**, 71 (5), 431–458.
- (48) Fanali, G.; di Masi, A.; Trezza, V.; Marino, M.; Fasano, M.; Ascenzi, P. Mol. Aspects Med. **2012**, 33 (3), 209–290.
- (49) Iwasaki, T.; Nakajima, K.; Hirowatari, Y.; Matsushita, M. Ann. Clin. Biochem. **2023**, 60 (5), 320–327.
- (50) Trivedu, V. D.; Saxena, I.; Siddiqui, M. U.; Qasim, M. A. *Biochem. Mol. Biol. Int.* **1997**, 43 (1), 1–8.